

3D Segmentation of Kidney Tumors from Freehand 2D Ultrasound

Anis Ahmad^{a,d}, Derek Cool^{b,d}, Ben H. Chew^c, Stephen E. Pautler^c and Terry M. Peters^{a,b,d}

^aGraduate Program in Biomedical Engineering

^bDepartment of Medical Biophysics

^cDivision of Urology, Department of Surgery

University of Western Ontario, London, ON, Canada

^dImaging Research Laboratories, Robarts Research Institute

100 Perth Drive, London, ON, Canada, N6A 5K8

ABSTRACT

To completely remove a tumor from a diseased kidney, while minimizing the resection of healthy tissue, the surgeon must be able to accurately determine its location, size and shape. Currently, the surgeon mentally estimates these parameters by examining pre-operative Computed Tomography (CT) images of the patient's anatomy. However, these images do not reflect the state of the abdomen or organ during surgery. Furthermore, these images can be difficult to place in proper clinical context. We propose using Ultrasound (US) to acquire images of the tumor and the surrounding tissues in real-time, then segmenting these US images to present the tumor as a three dimensional (3D) surface. Given the common use of laparoscopic procedures that inhibit the range of motion of the operator, we propose segmenting arbitrarily placed and oriented US slices individually using a tracked US probe. Given the known location and orientation of the US probe, we can assign 3D coordinates to the segmented slices and use them as input to a 3D surface reconstruction algorithm. We have implemented two approaches for 3D segmentation from freehand 2D ultrasound. Each approach was evaluated on a tissue-mimicking phantom of a kidney tumor. The performance of our approach was determined by measuring RMS surface error between the segmentation and the known gold standard and was found to be below 0.8 mm.

Keywords: Image-Guided Surgery, Ultrasound-based Segmentation

1. INTRODUCTION

Kidney cancer caused an estimated 12,660 deaths in 2005 in the United States, and an estimated 36,160 new cases in the same year.¹ Radical nephrectomy, the surgical removal of a diseased kidney and the surrounding fat tissues, is the preferred treatment for large tumors. Partial nephrectomy, resection of only the diseased tissue while leaving the remainder of the kidney, spares healthy nephrons and allows the patient to retain relatively good function of the affected kidney. The rate of cure for kidney cancer is not affected by removing the entire kidney or only part of it; therefore, the standard of care for tumors less than 4 cm is a partial nephrectomy.²⁻⁴ An ideal partial nephrectomy minimizes removal of the healthy nephrons in the kidney, while completely eliminating the tumor. Achieving this goal requires precise knowledge of the location of the tumor within the kidney.

Currently, surgeons are trained to carefully study pre-operative images obtained through either computed tomography (CT) or magnetic resonance imaging (MRI) to determine the boundary between the the tumor and the surrounding tissue. While effective, this approach is still challenging for a variety of reasons. In addition to having to visualize a three-dimensional structure from a series of two-dimensional images, this study requires the surgeon to memorize both the surface of the tumor, and any relevant anatomical features that would help guide and determine ideal points of entry for resection. Furthermore, the images obtained from pre-operative imaging do not necessarily reflect the state of the patient during surgery, as significant displacement of the kidney and surrounding organs occurs during surgery in order to expose the organ. Finally, the kidney is surrounded by a

Anis Ahmad: aahmad@imaging.robarts.ca

Terry M. Peters: tpeters@imaging.robarts.ca

protective layer of fat which obscures the view of the kidney during surgery. This fat must be left on the tumor to reduce the risk of tumor cells reseeding elsewhere in the body.

We believe an image-guided approach would improve the quality of laparoscopic partial nephrectomies. In particular, we propose using intra-operative ultrasound image-guidance to visually identify the location of the tumor to allow the surgeons to determine an optimal line of resection. Ultrasound provides rapid acquisition in a cost-effective system that is sufficiently small to be used in a laparoscopic procedure and is already employed intraoperatively during open and laparoscopic partial nephrectomies. Image-guidance is provided in the form of a three-dimensional surface model of the tumor, produced immediately before resection by segmenting US images acquired intra-operatively.

Ultrasound-based segmentation has been used effectively for a variety of anatomical systems. Of particular interest to our work are the ultrasound-based approaches to extracting 3D surfaces. In 2000, Abolmaesumi⁵ demonstrated the use of ultrasound in the extraction of carotid arteries from two-dimensional (2D) ultrasound images, while Ladak⁶ demonstrated the use of discrete dynamic contour (DDC) in segmenting ultrasound images of the prostate. The use of DDC's in prostate segmentation was further advanced by using the algorithm to produce three-dimensional (3D) segmentations. 3D segmentation is achieved either by generalizing the DDC algorithm,⁷ or by using the DDC on 2D slices extracted from 3D ultrasound images and arranging these segmented slices to represent the 3D segmentation.⁸⁻¹⁰

Also of interest are approaches that use existing knowledge of the shape to be segmented (shape priors) to improve segmentation results. Chen¹¹ proposed an extension to the DDC that evolves the contour towards an existing shape. Xie¹² analyzed existing images of the kidney to determine a basis of shapes that are used to represent additional kidneys, and a series of ultrasound images of the kidney to determine texture information that can help fit new kidney images to this basis. Gong¹³ employed a Bayesian framework to fit a simplistic model, a superellipse, to ultrasound images of the prostate.

We present an approach similar to those mentioned above to generate 3D segmentations of kidney tumors from freehand, tracked, 2D ultrasound. Furthermore, we introduced acquisition protocols that are feasible in surgical procedures where the ultrasound probe has limited mobility, such as laparoscopic surgeries, including one that uses prior knowledge of kidney tumor morphology. The remainder of the paper is organized as follows. In Section 2, we briefly review existing work. In Section 3, we describe our tumor segmentation method, and in sections 4 and 5 we describe experimental methods and demonstrate our results.

2. GEOMETRIC APPROACH TO ULTRASOUND SEGMENTATION

2.1. Discrete Dynamic Contour

The DDC method was first introduced by Lobregt and Viergever¹⁴ and was based on earlier work by Miller.¹⁵ This approach involves examining the neighbourhood surrounding each vertex on a contour and computing an energy function at the vertex. The energy function is designed such that the boundary of the object to be segmented coincides with a local minimum on the domain of the energy function. By analyzing the energy function at each vertex, a force can be computed that causes the vertex to travel towards the local minima. Thus, the contour evolves towards the ideal boundary of the object to be segmented. Conventional DDCs use energy functions that consist of factors that dampen velocity, minimize curvature and seek boundaries. The boundary is sought by evolving the contour towards parts of the image where a large discontinuity in the intensity values exist. However, this approach is difficult when segmenting real-world images due to the various sources of noise and unrelated intensity variations in the image.

Despite the difficulty in computing effective energy functions for images, Ladak demonstrated that DDCs may be used to segment ultrasound images.⁶ Using a sufficiently large Gaussian kernel to smooth the image prior to computing the energy function, one is able to overcome the numerous local minima that would otherwise appear in the energy function as a result of the speckle artifacts and other inhomogeneities in the image. Ladak's work treated the contour as a cubic function fit through four vertices. Ding¹⁶ elaborated on Ladak's approach by using piecewise cubic Cardinal splines, which permit the use of more than 4 points on the initial contour, allowing the spline to represent a greater range of shapes.

2.2. 3D Segmentation

Given the effectiveness of DDC's for 2D segmentation, they were naturally adapted for use in 3D segmentation as well. The logical approach is to simply increase the dimensionality and treat the contour as a closed set of connected points that defines a surface in \mathbb{R}^3 rather than defining a closed line in \mathbb{R}^2 . However, to increase the dimensionality, one needs to obtain a 3D ultrasound image to compute the energy functions at all vertices of the contour. While 3D ultrasound transducers exist, they are not suited for all imaging tasks and, in particular, are not as yet available as laparoscopic probes. Where 3D ultrasound devices are not available, 3D images are obtained by merging a series of contiguous 2D images obtained by either a mechanical¹⁷ or freehand¹⁸ acquisition. Ghanei⁷ demonstrated that by manually segmenting many of the 2D slices used to generate the 3D image, fitting a surface to these 2D contours and evolving the surface, accurate 3D segmentations could be generated.

Wang⁸ demonstrated that the DDC approach could be used to produce equally accurate 3D segmentations of the prostate without evolving a surface. In their work, slices were extracted from the 3D ultrasound image and segmented individually using a DDC. Two methods for slice-based segmentation were considered: parallel reslicing, which employs a contiguous set of parallel slices, but suffers from poorer segmentations; and rotational reslicing, which acquires slices rotated around a medial axis through the prostate. The slice-based approach attained segmentation times on the order of seconds, since evolving a 2D contour is more efficient than evolving a 3D isosurface. Furthermore, the authors only manually seeded one slice and used the resulting segmentation of each slice to seed subsequent slices. Once all the slices are segmented, a series of contours exist where each contour lies approximately on the surface of the prostate. These contours were then used to represent a 3D model of the prostate.

Slice-based approaches have many benefits for providing image guidance in partial nephrectomies. The speed at which they execute is important as the surgeons have a fixed amount of time to perform the resection since the blood supply to the kidney is blocked during the procedure. The use of 2D slices is important since it allows the use of traditional 2D ultrasound probes, including laparoscopic probes. However, relying on the presence of an image volume is problematic in laparoscopic procedures where the access ports limit the size of any tool entering the body, thus preventing most mechanical means for 3D ultrasound acquisition. Also, the mobility of the tools is constrained by both the limited number of access ports in laparoscopic procedures, and by the fact that the surgeons must lay the transducer on the surface of the kidney since the pressurized CO₂ (employed to create a working space in the abdomen) prevents all but direct sonic access to the kidney. Finally, it is challenging to obtain the rotational slices as proposed by Wang⁸ with the mobility constraints described. Instead, we propose two acquisition protocols that permit a small number of slices to be acquired with relatively arbitrary orientations.

3. KIDNEY TUMOR SEGMENTATION FROM FREE-HAND ULTRASOUND

3.1. Unguided Kidney Tumor Segmentation

We employed a modified form of Cool's method that acquired slices directly from freehand 2D ultrasound. We place a six degree-of-freedom optical tracker on the ultrasound transducer, which allows us to determine the position and orientation of the ultrasound image in 3D world coordinates at all times. We obtain sweeps of the kidney, either by rotating the probe about the transducer, or by moving the transducer along the surface of the kidney. While sweeping, our system records an ultrasound image and its corresponding tracking information every time the transducer has moved. In order to prevent oversampling of the tumor, we only acquire a new slice if the transducer has either been displaced by at least 2.5 mm or has been rotated at least 5 degrees. Once the sweep is complete, the first acquired image is presented to the user, who selects a minimum of 4 tumor boundary points, which are then fitted with a Cardinal spline.¹⁶ This contour is refined as a DDC, then used as a seed for the next image. The algorithm then refines the DDC on the new image and permits the user to further refine the contour, if needed. This propagation of contours continues for the remaining images in the sweep. The generated contours are sampled, and the sample points are stored. The user may then choose to obtain additional sweeps until the user is satisfied that a sufficient images have been acquired. When all slices have been acquired and contoured, they are further processed by a surface reconstruction algorithm¹⁹ that generates

the segmented surface. To help determine when sufficient sweeps have been made, we fit a surface to the existing sampled points and display it after each sweep.

3.2. Guided Kidney Tumor Segmentation

Renal-cell carcinomas generally produce tumors that are spherical or egg-shaped.²⁰ We may use this information to guide the three-dimensional segmentation of the tumor by permitting fewer slices to be obtained and by only requiring the user to manually segment one contour (see figure 1 for an illustration of the guided tumor segmentation approach). The symmetry present in spheres and ovoids permits us to compute an approximate representation of the tumor after segmenting only one ultrasound slice. The guided approach begins by acquiring an initial ultrasound slice of the tumor, such that the slice plane is approximately coincident with the major axis of the ovoid tumor. Once this slice is acquired, the user manually identifies the boundary as in the previous section. The spline is parameterized using the euclidean distance between each pair of spline points. We use this parameterization as it allows us to generate a contour defined by approximately equidistant points. Once the contour is refined using the DDC method, the equidistant distribution of points is used to estimate the center of mass by averaging the points on the contour. We estimate the major axis of the ovoid by performing a principle components analysis (PCA) of the point set. The PCA returns the principle axes of the point set, with the major axis corresponding to the eigenvector with the largest corresponding eigenvalue. We now take the contour and rotate it around the major axis N times in increments of π/N , similar to Wang's rotational reslicing.⁸ The points generated along the rotated contours are fed into the surface-fitting algorithm¹⁹ which creates what we refer to as a guide surface.

The guide surface is not intended to be a segmentation of the tumor. Rather it is used to guide the creation of seed contours. Once the guide surface is created, the user continues to acquire arbitrary tracked ultrasound slices. Upon acquisition, our algorithm computes the intersection between the ultrasound slice's plane and the guide surface, resulting in closed 2D contour. This contour is treated as a DDC that is refined according to the acquired image, then stored. The user continues to acquire images in this manner until satisfied with the number of acquisitions at which point the guide surface is discarded and the stored contours are fed into the surface fitting algorithm to generate the segmented surface of the tumor. As in the unguided approach, we present a surface fitted to the existing points stored after each acquisition to help the user determine whether further acquisitions are required.

Since the guide surface is not an exact representation of the tumor, there will be occasions when the ultrasound plane intersects the tumor, but not the guide surface. If the slice does not intersect the guide surface, no seeding contour will be produced for that slice and thus no contour will exist. The slice plane, however, would only miss the guide surface when it is roughly tangential to the surface of the tumor. As noted by Wang,⁸ images of tangential slices are challenging to segment accurately. Thus, the occasional inability to segment a tangential slice of the tumor will likely not detract appreciably from the utility of the method.

4. EXPERIMENTAL EVALUATION: METHODS

4.1. Validation methodology

We validate our approach by comparing the results of the segmented surface to that of a gold-standard surface. We do so by creating a tissue-mimicking phantom, as described below. The phantom was imaged by MRI with a 1.5T GE Signa scanner using a 3D SPGR sequence with an isotropic voxel size of 1mm. The resulting image was manually segmented on two occasions by the same individual, but with opposite orderings of the slices. The segmented images were averaged and the surface was extracted. The extracted surface was then used as the gold-standard for validation. All ultrasound images were acquired from an Aloka SSD-1700 ultrasound scanner, and the surfaces were fit using the FastRBF (FarField Technology Ltd., Christchurch, NZ) software package. To validate against the gold-standard, we rigidly registered the segmented surface to the gold-standard using the iterative closest point (ICP) algorithm. We computed the RMS error with the Hausdorff distance metric using the M.E.S.H. software.²¹

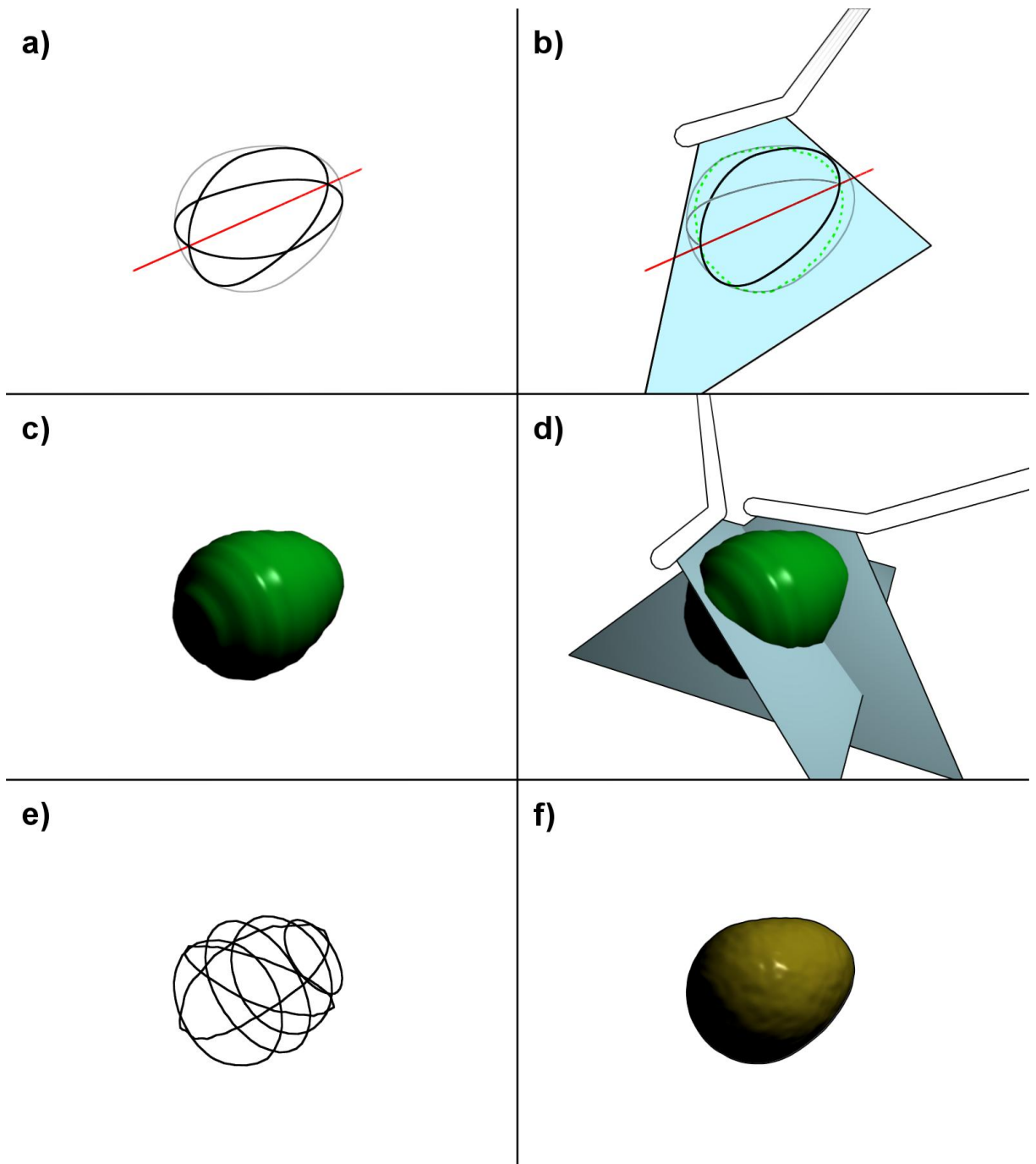


Figure 1. Demonstration of the guided segmentation approach. a) An ovoid shape, with the major axis in red. b) A laparoscopic ultrasound transducer acquiring an image through the major axis with the object contour segmented and shown as a green dotted line. c) The result of spinning the segmented contour around the major axis, producing the guide surface. d) The guide surface continuing to be imaged arbitrarily. e) Resulting contours from the numerous acquisitions. f) Resulting segmented surface.

4.2. Tissue-Mimicking Phantom

We used poly(vinyl alcohol) cryogel (PVA-C) as the tissue-mimicking material for our phantom. PVA-C has imaging characteristics suitable for mimicking tissue in both ultrasound and magnetic resonance imaging, and its imaging characteristics may be controlled by the number of times the PVA-C is frozen and thawed.²² We first filled a mould of an elongated sphere, roughly 5cm by 3cm, with PVA-C and froze it to -20°C for 24 hours. After thawing, the PVA-C tumor phantom was placed in a larger mould, the mould was then filled with fresh PVA-C gel and frozen again for 24 hours. The resulting phantom consisted of a PVA-C tumor phantom that underwent two freeze-thaw cycles, embedded in a larger mass of PVA-C that underwent one freeze-thaw cycle. The difference in the number of freeze-thaw cycles provided sufficient contrast between the tumor phantom and the surrounding material, and mimicked contrast seen in US images of actual kidney tumors. While the relative echogenicity of the tumor phantom and the surrounding material may be inverse to that found in real images, this would not affect our results since the DDC seeks out edges in the image represented by intensity discontinuities, and is invariant to the direction of the gradient at these edges.

5. EXPERIMENTAL EVALUATION: RESULTS

5.1. Unguided Segmentation Results

To validate the effectiveness of the unguided approach, we segmented the phantom using two sweeps: one translational sweep along the length of the phantom, and one rotational sweep about transducer. Nearly 20 individual images were acquired as a result. Most of the acquired images required manual editing of at least two points due to the contour being propagated incorrectly between frames. The results of comparing the segmented surface to the gold-standard are listed in table 1 and can be viewed in figure 2.

Table 1. Results of measuring the Hausdorff distance from the unguided segmented mesh to the gold standard.

Minimum	Maximum	Mean	Mean of Absolute	RMS	Standard Deviation
-2.47	1.58	-0.04	0.57	0.72	0.44

5.2. Guided Segmentation Results

To validate the effectiveness of the guided approach, we segmented the phantom using fewer than 10 arbitrarily oriented slices. The guide surface was able to produce seed contours that, once refined as a DDC, yielded good segmentations of each acquired image. Minimal manual re-editing was required, with the exception of slices that grazed the surface of the phantom. The guide surface can be seen in figure 3. Examples of the automatically generated seeds are shown in figure 4. The results of comparing the segmented surface to the gold-standard are listed in table 2 and can be viewed in figure 5.

Table 2. Results of measuring the Hausdorff distance from the guided segmented mesh to the gold standard.

Minimum	Maximum	Mean	Mean of Absolute	RMS	Standard Deviation
-2.61	2.17	-0.04	0.64	0.79	0.47

6. DISCUSSION

We have demonstrated efficient and accurate 3D segmentations of model kidney tumors using freehand 2D ultrasound. We attained superior results with the unguided approach, likely due to the fact that more images were acquired throughout the phantom. However, this additional accuracy came at the expense of additional manual editing on the part of the user. The guided approach, with little additional error, was able to segment

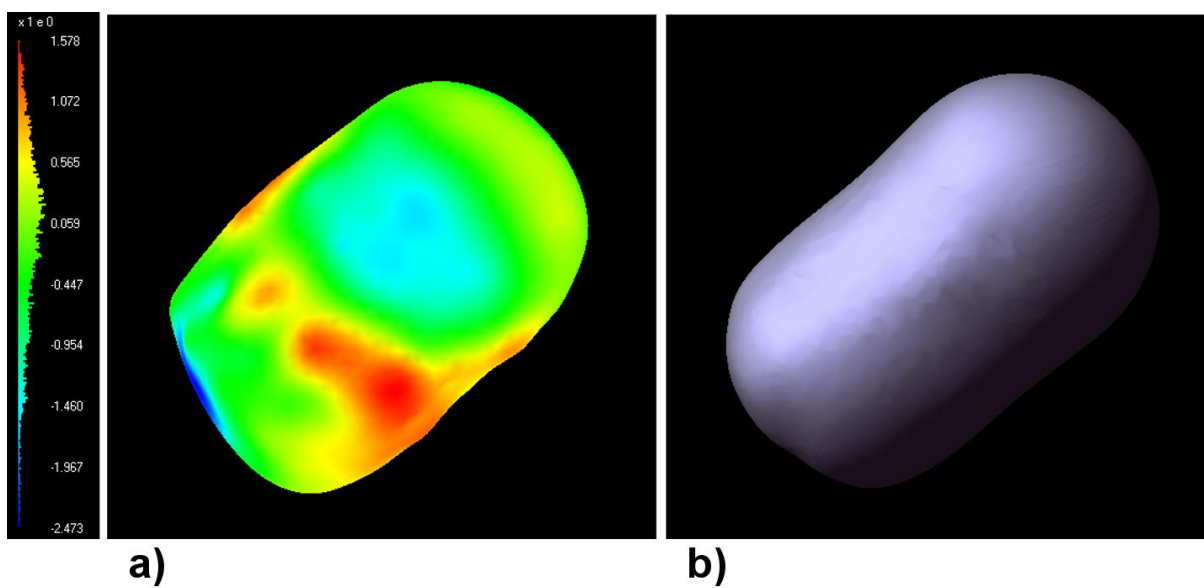


Figure 2. a) the unguided segmented surface color-mapped to indicate surface error, with green implying minimal error. b) the gold standard surface.

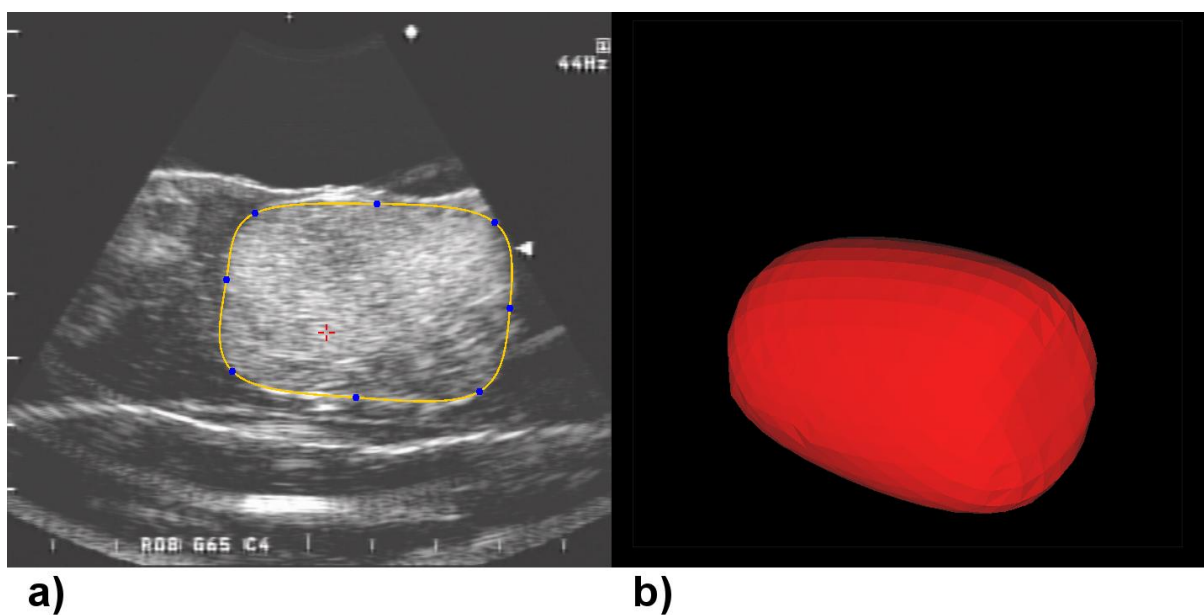


Figure 3. a) the image slice acquired and segmented. b) the guide surface generated from the segmented image.

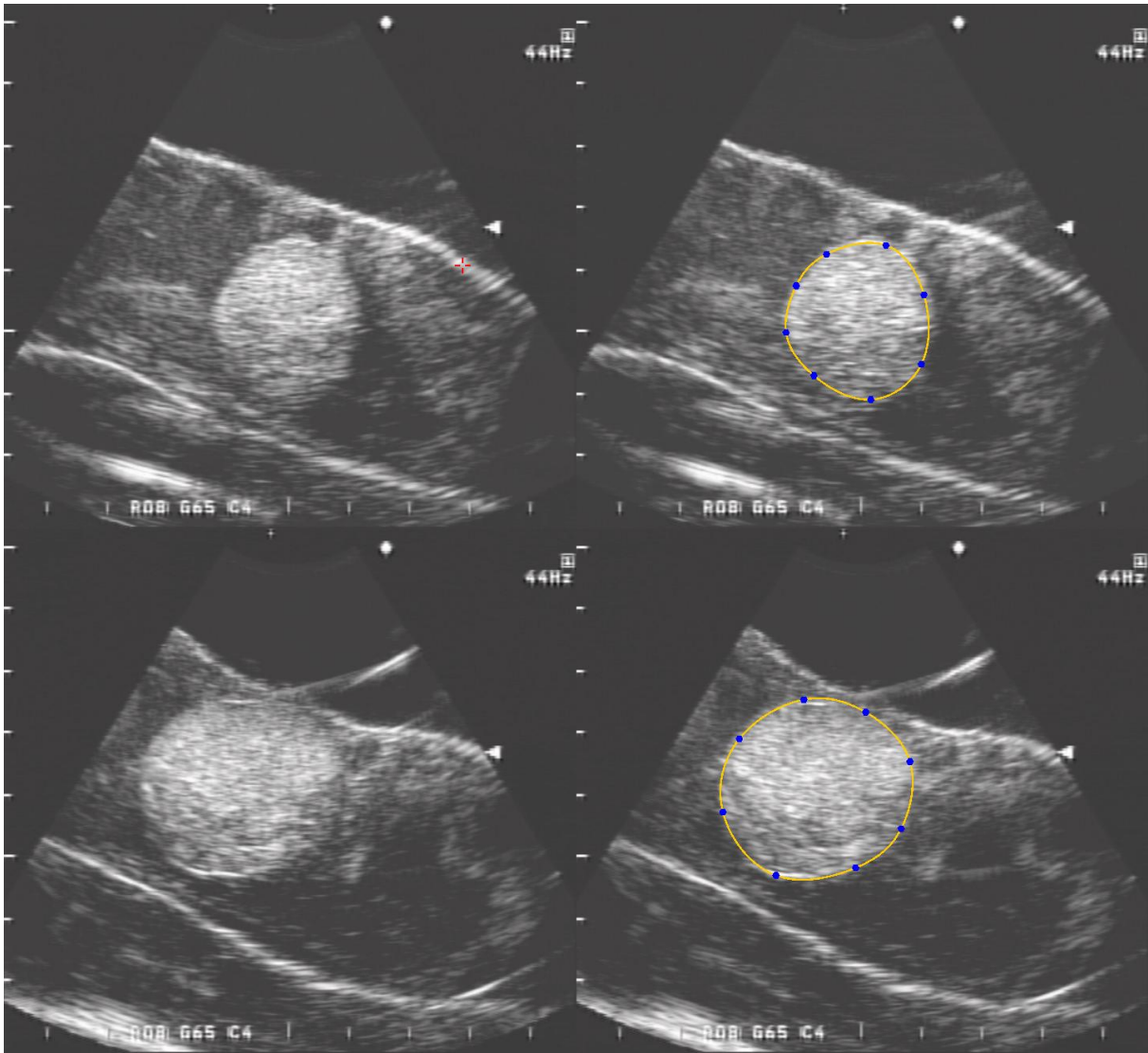


Figure 4. Examples of slices acquired arbitrarily through the phantom. The left column shows the slice acquired, and the right column shows the contour generated automatically using the guide surface.

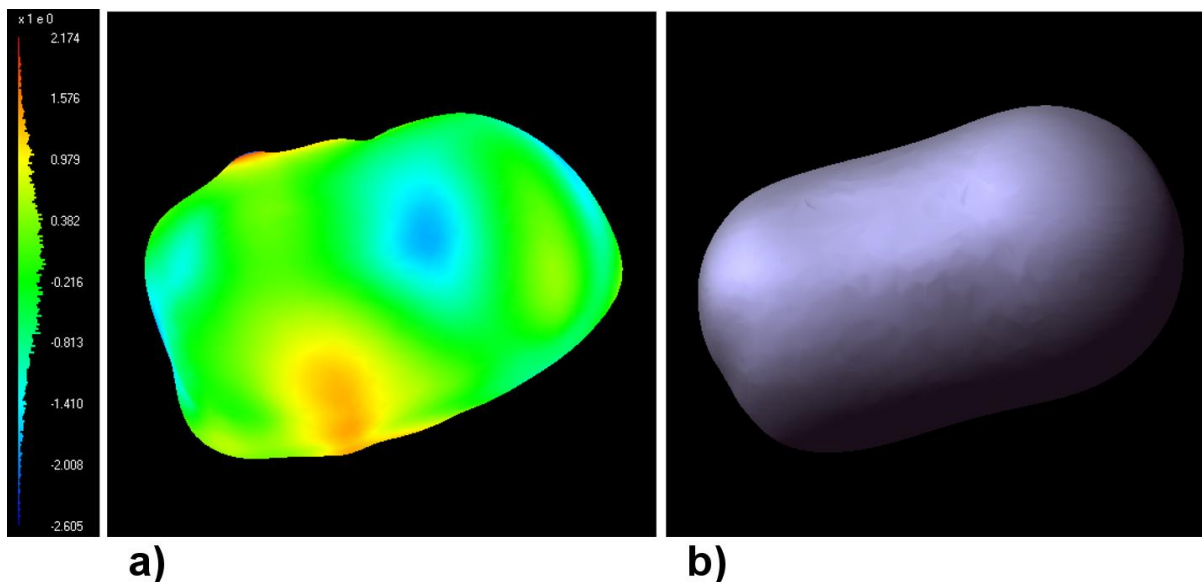


Figure 5. a) the guided segmented surface color-mapped to indicate surface error, with green implying minimal error. b) the gold standard surface.

the surface accurately with considerably less user effort. However, while the RMS distance from both approaches is below 0.8 mm, we should note that the minimum distance is roughly 2.5 mm for both approaches. This is a clinically relevant measure as it indicates how much the segmented surface underestimates the tumor's surface, which could cause a surgeon to resect into the tumor.

It should be noted that the phantom used to validate the approach was a little larger, at 5cm in length, than tumors found clinically in laparoscopic partial nephrectomies. However, the bulk of the images acquired were along the width of the phantom, which at 3cm is still clinically relevant. It should also be noted that this approach is designed for relatively homogeneous renal cell carcinomas, and would not necessarily be as effective in more heterogeneous lesions, such as cystic renal cell carcinomas, without using a more sophisticated segmentation technique that relies on more than local image intensity discontinuities.

Although the initial results of this work are promising, there is much work to be done to improve accuracy and usability of this approach. More sophisticated energy functions may make the DDCs more robust in ultrasound images. Improved methods for propagating contours in the unguided approach may reduce the amount of manual editing required. Automated segmentation algorithms may reduce the need for user participation dramatically. More powerful techniques, such as level sets, may be used to adapt this approach to segmenting structures with more geometric complexity. Mesh post-processing could be used to smooth the mesh further and remove concavities, in hopes of reducing underestimations of the tumor's surface. Finally, to complete image-guidance, we need to present the segmented surface to the surgeon in a clinically relevant manner. In the future, we intend to accomplish this by combining the segmented surface with tracked endoscopic images.

ACKNOWLEDGMENTS

The authors would like to thank Chris Wedlake, Marcin Wierzbicki, Ting Guo, John Moore, and Dr. David Gobbi for their assistance throughout this project. Funding has been provided by the Natural Sciences and Engineering Research Council of Canada, the Canadian Institutes of Health Research (MOP 62716), and the Canadian Foundation for Innovation.

REFERENCES

1. American Cancer Society. http://www.cancer.org/docroot/LRN/LRN_0.asp?dt=22, 2005.
2. A. Finelli and I. Gill, "Laparoscopic partial nephrectomy: contemporary technique and results," *Urologic Oncology* **22**, pp. 139–144, 2004.
3. I. Gill, S. Matin, M. Desai, J. Kaouk, A. Steinberg, E. Mascha, J. Thornton, M. Sherief, B. Strzempkowski, and A. Novick, "Comparative analysis of laparoscopic versus open nephrectomy for renal tumors in 200 patients," *Journal of Urology* **170**, pp. 64–68, 2003.
4. S. Matin, I. Gill, S. Worley, and A. Novick, "Outcome of laparoscopic radical and open partial nephrectomy for the sporadic 4cm. or less renal tumor with a normal contralateral kidney," *Journal of Urology* **168**, pp. 1356–1359, 2002.
5. P. Abolmaesumi, M. R. Sirouspour, and S. E. Salcudean, "Real-time extraction of carotid artery contours from ultrasound images," in *Computer-Based Medical Systems*, pp. 181–186, 2000.
6. H. M. Ladak, F. Mao, Y. Wang, D. B. Downey, D. A. Steinman, and A. Fenster, "Prostate boundary segmentation from 2D ultrasound images," *Med Phys.* **27(8)**, pp. 1777–88, 2000.
7. A. Ghanei, H. Zadeh, A. Ratkewicz, and F. Yin, "Semiautomatic three-dimensional segmentation of the prostate using two-dimensional ultrasound images," *Med. Phys.* **28(10)**, pp. 2147–2153, 2001.
8. Y. Wang, H. N. Cardinal, D. B. Downey, and A. Fenster, "Semiautomatic three-dimensional segmentation of the prostate using two-dimensional ultrasound images," *Med Phys.* **30(5)**, pp. 887–97, 2003.
9. M. Ding, I. Gyacskov, X. Yuan, M. Drangova, and A. Fenster, "Slice-based prostate segmentation in 3D US images based on continuity constraint," in *SPIE Medical Imaging 2004: Visualization, Image-Guided Procedures and Display*, **5367**, pp. 151–158, 2004.
10. D. Cool, D. Downey, T. Peters, and A. Fenster, "3D prostate model reconstruction from 2D transrectal ultrasound biopsy images," *Med Phys.* **32(6)**, p. 2154, 2005.
11. Y. Chen, S. Thiruvankadam, H. Tagare, F. Huang, D. Wilson, and E. Geiser, "On the incorporation of shape priors into geometric active contours," in *Proceedings of the IEEE Workshop on Variational and Level Set Methods in Computer Vision 2001*, pp. 145–152, 2001.
12. J. Xie, Y. Jiang, and H. Tsui, "Segmentation of kidney from ultrasound images based on texture and shape priors," *IEEE Transactions on Medical Imaging* **24(1)**, pp. 45–57, 2005.
13. L. Gong, S. Pathak, D. Haynor, P. Cho, and Y. Kim, "Prostate segmentation in ultrasound images with deformable shape priors," in *SPIE Medical Imaging: Visualization, Image-Guided Procedures, and Display*, R. L. Galloway, ed., **5029**, pp. 535–543, 2003.
14. S. Lobregt and M. Viergever, "A discrete dynamic contour model," *IEEE Transactions on Medical Imaging* **14(1)**, pp. 12–24, 1995.
15. J. Miller, D. Breen, W. Lorensen, R. O'Bara, and M. Wozny, "Geometrically deformable models: A method to extract closed geometric models from volume data," in *Proceedings of SIGGRAPH 1991*, pp. 217–226, ACM Press, 1991.
16. M. Ding, C. Chen, Y. Wang, I. Gyacskov, and A. Fenster, "Prostate segmentation in 3D US images using the cardinal-spline based discrete dynamic contour," in *SPIE Medical Imaging 2003, Visualization, Image-Guided Procedures, and Display*, **5029**, pp. 69–76, 2003.
17. A. Fenster, S. Tong, S. Sherebrin, D. Downey, and R. Rankin, "Three-dimensional ultrasound imaging," in *SPIE Medical Imaging 1995: Physics of Medical Imaging*, R. van Metter and J. Beutel, eds., **2432**, pp. 176–184, 1995.
18. D. G. Gobbi and T. M. Peters, "Interactive intra-operative 3D ultrasound reconstruction and visualization," in *Part II, Proceedings of MICCAI*, T. Dohi and R. Kikinis, eds., *Lecture Notes in Computer Science* **2489**, pp. 156–163, Springer, 2002.
19. J. Carr, R. Beatson, J. Cherrie, T. Mitchell, W. Fright, B. McCallum, and T. Evans, "Reconstruction and representation of 3D objects with radial basis functions," in *Proceedings of SIGGRAPH 2001*, pp. 67–76, ACM Press, 2001.
20. P. C. Walsh, A. B. Retik, E. D. Vaughan, A. J. Wein, L. R. Kavoussi, A. C. Novick, A. W. Partin, and C. A. Peters, eds., *Campbell's urology, 8th edition*, vol. 4. Saunders, 2002.

21. N. Aspert, D. Santa-Cruz, and T. Ebrahimi, "Mesh: Measuring errors between surfaces using the hausdorff distance," in *Proceedings of the IEEE International Conference on Multimedia and Expo*, **I**, pp. 705–708, 2002. <http://mesh.epfl.ch>.
22. K. Surry, H. Austin, A. Fenster, and T. Peters, "Poly(vinyl alcohol) cryogel phantoms for use in ultrasound and MR imaging," *Physics in medicine and biology* **49(24)**, pp. 5529–5546, 2004.